PHYSICAL REVIEW B VOLUME 46, NUMBER 7 15 AUGUST 1992-I

Electronic structure of 3d-transition-metal compounds by analysis of the 2p core-level photoemission spectra

A. E. Bocquet*
Department of Applied Physics, University of Tokyo, Bunkyo-ku, Tokyo 113, Japan

T. Mizokawa, T. Saitoh, H. Namatame, and A. Fujimori†
Department of Physics, University of Tokyo, Bunkyo-ku, Tokyo 113, Japan

(Received 26 September 1991)

The electronic structures of a wide range of transition-metal compounds, including Cu, Ni, Co, Fe, and Mn oxides and sulfides, with metal valences ranging from 2+ to 4+, have been investigated by a cluster-type configuration-interaction analysis of the core-level 2p x-ray photoemission spectra. We show that by including the d-d exchange interaction (retaining only diagonal terms) and an anisotropic metal-ligand hybridization in the model, these spectra can be well reproduced, and so can be used to deduce quantitatively values for the ligand-to-metal charge-transfer energy Δ, the on-site d-d Coulomb repulsion energy U, and the metal-ligand transfer integrals T. Systematics for Δ and U are generally consistent with those found from previous valence-band studies and follow expected chemical trends. By using values of Δ and U found from this model, we show that most of the transition-metal compounds studied in this work can be classified in the charge-transfer regime of the Zaanen-Sawatzky-Allen diagram. A few exceptions to these systematics have been found. Small U values found for pyrite-type CoS_2 and FeS_2 and large T values for Mn perovskite oxides, as well as the neglect of other mechanisms such as exciton satellites, may indicate a limitation of the local-cluster model.

I. INTRODUCTION

Transition-metal (TM) compounds, particularly oxides, sulfides, and halides, have been the subject of numerous experimental and theoretical studies because of the breakdown in the use of one-electron band-structure calculations to describe their electronic and physical properties. Recently, a reinterpretation of photoemission spectroscopy data[1], and the discovery of high-temperature superconductivity in copper oxides[2] have revived interest in a fuller understanding of the electronic structure of these compounds.

Studies of simple divalent TM monoxides, such as MnO, CoO, NiO, and CuO,[3-6] have shown that the band gaps of the insulating oxides of the late transition metals are of a charge-transfer type, defined by a ligand-to-metal charge-transfer energy Δ, where $\Delta < U$, the on-site d-d Coulomb interaction energy. This differs from the case of the early TM oxides, where $U < \Delta$ and a Mott-Hubbard-type d-d band gap is formed. The failure of one-electron theory to describe the electronic structure of the late TM compounds results from the high-energy nature of the d-d Coulomb interactions which dominate over the bandwidth to such an extent that an independent-electron description breaks down. One useful microscopic probe of these high-energy interactions is core-level photoemission spectroscopy, in which the screening response of the valence electrons to the sudden creation of a core hole is probed.

The appearance of strong satellite structure accompanying the main peaks in the metal 2p core-level x-ray photoemission spectra (XPS) of TM compounds is well known.[7] Systematic variations in the positions and intensities of these satellites, depending on the chemical nature of the compound, suggest that they may provide important clues · to understanding the electronic structure. Indeed, a proper interpretation of the 4f core-level satellites of insulating rare-earth compounds has provided a wealth of information on the valence-level electronic structure of these compounds.[8] Although various models have been proposed for the occurrence of 2p core-level XPS satellites,[9-12] it must be stressed that any attempt at a quantitative interpretation must account for the many-body nature of the correlated valence electrons. Early attempts based on the so-called "shakeup" of a valence electron accompanying photoionization[10,11] were based on an independent-electron picture for the valence electrons and failed to satisfactorily explain the origin of the satellite structure.

An attempt to give a quantitative interpretation of the core-level spectra using a configuration-interaction approach was made by van der Laan *et al.*[13] following earlier work by Larsson.[14] A charge-transfer model using an impurity-type configuration-interaction Hamiltonian and explicitly taking into account the Coulomb attraction between the core hole and localized valence electrons and the resulting charge-transfer screening response was used to describe the 2p XPS spectrum of the insulating Cu^{2+} dihalides (d^9 configuration). The physics could be described in terms of a few parameters, namely, the d-d Coulomb repulsion energy U, the charge-transfer energy Δ, the ligand-p–metal-d hybridization energy T, and the core-hole–d-electron Coulomb attraction energy Q. The screening or relaxation process of the valence electrons in the XPS final state, where a core hole is created, means that even for the insulating Cu^{2+} dihalides, the lowest-energy final state is a screened state.[14] Thus, they proposed that the main peak in the Cu 2p XPS spectrum was due to a $\underline{c}3d^{10}\underline{L}$ configuration and the satellite at higher binding energy was due to a $\underline{c}3d^{9}$ configuration, where $\underline{c}$ and $\underline{L}$ represent a core and a ligand hole, respectively. This is in contrast to earlier models where the final state corresponding to the main peak had the same valence configuration as the initial ground state.[11]

This model was successfully extended by Zaanen, Westra, and Sawatzky[15] to the Ni^{2+} dihalides, where they found that for parameter values in this range, a cluster-type calculation served as a good approximation to the full impurity-type calculation. Further work by Park *et al.*[16] using the cluster-type approach applied the model to lighter TM dihalides (CoX_2, FeX_2, and MnX_2). The fact that both the intensities and the positions of the 2p XPS satellites could be reproduced using parameter values which followed expected chemical trends showed that a many-body configuration-interaction approach is necessary in order to understand the spectra. However, parameter values obtained in this way do not necessarily agree with those found from valence-band[3-6] and 2p x-ray absorption (XAS) (Ref. 17) studies. It has been unclear so far as to whether these discrepancies are due to simplifications made on the model or to additional effects caused by the presence of a core hole in the final state.

In this work we extend the charge-transfer model of van der Laan *et al.*;[13] Zaanen, Westra, and Sawatzky;[15] and Park *et al.*[16] by including the d-d exchange interaction and an anisotropic hybridization effect to investigate the electronic structure of a wide range of TM compounds, including Cu, Ni, Co, Fe, and Mn oxides and sulfides with metal valences ranging from 2+ to 4+. We thus find excellent agreement between theory and experiment for most of the spectra with best-fit parameters for Δ and U following expected chemical trends. Parameters obtained from the core-level XPS spectra also compare well with those learned from previous studies of the valence bands, although the present analysis requires much less computational effort. The success of the present model calculations using parameters close to those used to explain the valence band gives us confidence that such a model can be used to study the valence-electronic structure of the late TM compounds in more detail than has been done previously.

II. MATERIALS AND EXPERIMENTAL DETAILS

The TM compounds studied in this work include divalent monoxides (NiO, FeO, and MnO), sulfides (NiS, $Zn_{0.5}Mn_{0.5}S$), disulfides (NiS_2, CoS_2, and FeS_2), and intercalation compounds ($Ni_{0.33}TiS_2$, $Fe_{0.33}TiS_2$, $Mn_{0.25}TiS_2$); trivalent α-Fe_2O_3 and $NaCuO_2$; and trivalent or tetravalent perovskite oxides ($LaFeO_3$, $SrFeO_3$, $LaMnO_3$, and $SrMnO_3$). For each TM compound apart from $Zn_{0.5}Mn_{0.5}S$, the central TM cation is located in an ideal or distorted octahedron formed by the nearest-neighboring six ligands. The small distortions are usually of tetragonal or rhombohedral type and can be ignored for our purposes. The intercalation compounds form layered structures with the guest TM cation located between alternating TiS_2 blocks.[18] The local environment of the cation is similar to that of NiS, with the cation octahedrally coordinated to six S ligands which form hexagonal-close-packed structures. $Zn_{0.5}Mn_{0.5}S$ has a zinc-blende structure with the TM cation tetrahedrally coordinated to four S ligands.[19] This compound can be considered within the same model as the octahedral compounds if appropriate modifications are made to reflect the changes in the transfer integrals between the ligand-p and metal-d orbitals. The disulfides have pyrite-type structures in which the TM cation is octahedrally coordinated by six $(S_2)^{2-}$ molecules.[20] Formally trivalent $NaCuO_2$ consists of square-planar CuO_2 ribbons and forms a layered structure.[22] Here, we can simply ignore the $d_{3z^2-r^2}$ orbital since two holes are present in the $d_{x^2-y^2}$ orbital in the ground state. Some preparation details of these materials have been reported elsewhere,[3,18,20-26] with single-crystal samples being obtained for NiO, NiS_2, CoS_2 Fe_2O_3, MnO, $Zn_{0.5}Mn_{0.5}S$, and the intercalation compounds.

According to ligand field theory, the 3d level in an octahedral crystal field splits into a low-lying t_{2g} triplet and a higher-lying e_g doublet, separated by the crystal-field splitting, 10Dq. The ionic ground-state configurations for the TM cations range from d^3 for Mn^{4+} to d^8 for Ni^{2+} and Cu^{3+}. All configurations are in a high spin state[25,27] except for FeS_2 and CoS_2 where the d electrons are in a low spin state. Square-planar d^8 $NaCuO_2$ is also in a low spin state. The ground-state electronic configurations are listed in more detail in Table I.

Core-level 2p XPS spectra were obtained using a spectrometer equipped with a Mg $K\alpha$ source ($h\nu = 1253.6$ eV) and a double-pass cylindrical mirror analyzer with a resolution of ≈ 1 eV. Some measurements were also performed separately on an instrument equipped with an Al $K\alpha$ source ($h\nu = 1486.6$ eV). Clean surfaces were obtained by scraping *in situ* with a diamond file within the spectrometer chamber with a base pressure of $\approx 1\times10^{-10}$ Torr. All measurements were performed at room temperature except for the ternary oxides. These compounds were measured at liquid nitrogen temperatures (≈ 80 K) as they have a tendency to lose oxygen from the surface region under ultrahigh-vacuum conditions. All spectra have been corrected for satellites arising from the x-ray source and for the kinetic-energy dependence of the analyzer transmission efficiency. Variable charging shifts were detected for the insulating compounds so absolute binding energies are not considered here. Bulk-plasmon satellites accompanying the metal $2p_{3/2}$ peak were also detected in most spectra on the high-binding-energy side of the metal $2p_{1/2}$ peak. Some of these spectra have been published previously.[18,22,24,25]

The subtraction of the secondary-electron background was found to be a nontrivial problem, as deduced parameter values were found to vary according to the height of the subtracted background. Proportional coefficients for the integral background were determined from other core levels of the same compound which showed no charge-

TABLE I. Ground-state electronic configurations, local moments, and the number of basis states used to describe the Hamiltonian for each configuration of the TM ions studied. Also included are Racah parameters (in eV) B and C, for these ions, taken from Ref. 30. HS indicates a high-spin configuration, while LS indicates a low-spin configuration.

TM ion (spin state)	Ground-state configuration	Local moment, S	Number of basis states	Racah parameters B	C
Mn^{4+} (HS)	$t_{2g\uparrow}^3$	$\frac{3}{2}$	36	0.132	0.610
Mn^{3+} (HS)	$t_{2g\uparrow}^3 e_{g\uparrow}$	2	24	0.120	0.552
Fe^{4+} (HS)	$t_{2g\uparrow}^3 e_{g\uparrow}$	2	24	0.138	0.645
Mn^{2+} (HS)	$t_{2g\uparrow}^3 e_{g\uparrow}^2$	$\frac{5}{2}$	12	0.107	0.477
Fe^{2+} (HS)	$t_{2g\uparrow}^3 e_{g\uparrow}^2$	$\frac{5}{2}$	12	0.126	0.595
Fe^{2+} (HS)	$t_{2g\uparrow}^3 t_{2g\downarrow} e_{g\uparrow}^2$	2	9	0.114	0.500
Fe^{2+} (LS)	$t_{2g\uparrow}^3 t_{2g\downarrow}^3$	0	9	0.114	0.500
Co^{2+} (LS)	$t_{2g\uparrow}^3 t_{2g\downarrow}^3 e_{g\uparrow}$	$\frac{1}{2}$	6	0.120	0.558
Ni^{2+} (HS)	$t_{2g\uparrow}^3 t_{2g\downarrow}^3 e_{g\uparrow}^2$	1	3	0.128	0.601
Cu^{3+} (LS)[a]	$t_{2g\uparrow}^3 t_{2g\downarrow}^3 e_{g\uparrow} e_{g\downarrow}$	0	4	0.144	0.717

[a] The two e_g holes are in the x^2-y^2 symmetry orbits.

transfer satellites, and integral backgrounds determined from these coefficients were then subtracted from the metal-cation $2p$ core-level spectra.

III. CLUSTER-TYPE CHARGE-TRANSFER MODEL CALCULATION

We now present an extension of the models of van der Laan *et al.*;[13] Zaanen, Westra, and Sawatzky;[15] and Park *et al.*[16] to investigate the electronic structure of a wide range of TM compounds using a configuration-interaction approach. We use a cluster-type calculation in which the ligand bandwidth is approximated to be zero. The cluster approximation has been found to be a good first-order approximation to the full impurity-model calculation, with the physics being described in terms of only a few parameters, namely, U, Δ, T, and Q. This means that calculated spectra can be simply fitted to experimental data by the manipulation of these parameters.

In the cluster approximation, we consider an idealized structure with the central metal cation surrounded by an octahedron (a tetrahedron for $Zn_{0.5}Mn_{0.5}S$) of anions. The ground state of the formally d^n ion is described as a mixture of the purely d^n-ionic state and screened $d^{n+1}\underline{L}$, $d^{n+2}\underline{L}^2$, etc., charge-transfer states in which one or more electrons are transferred to the $3d$ levels from the neighboring ligand p orbitals:

$$\Psi_g = a_0|d^n\rangle + \sum_m a_m|d^{(n+m)}\underline{L}^m\rangle \ . \tag{1}$$

For the TM compounds under consideration, $n = 3,4,\ldots,8$, and the right-hand side is summed over the number of $\underline{L}$ ligand holes $m = 1,2,\ldots,10-n$. Crystal-field effects and the d-d exchange interaction are introduced by extending the basis set to discriminate between $t_{2g\uparrow\downarrow}$ and $e_{g\uparrow\downarrow}$ symmetry states. Equation (1) is, then,

$$\begin{aligned}\Psi_g &= a_0|(t_{2g\uparrow})^3(t_{2g\downarrow})^{n'_1}(e_{g\uparrow})^{n_2}(e_{g\downarrow})^{n'_2}\rangle \\ &+ \sum_{m'_1,m_2,m'_2} a_{m'_1 m_2 m'_2}|(t_{2g\uparrow})^3(t_{2g\downarrow})^{(n'_1+m'_1)}(e_{g\uparrow})^{(n_2+m_2)}(e_{g\downarrow})^{(n'_2+m'_2)}(\underline{L}_{\pi\uparrow})^{m'_1}(\underline{L}_{\sigma\downarrow})^{m_2}(\underline{L}_{\sigma\uparrow})^{m'_2}\rangle \ ,\end{aligned} \tag{2}$$

where $n'_1 = 1,2,3$ and $n_2, n'_2 = 1,2$, and the right-hand side is implicitly summed over all combinations of m'_1, m_2 and m'_2. Here, $n = (n'_1 + n_2 + n'_2 + 3)$ and m'_1, m_2, and m'_2 indicate the number of $\underline{L}_{\pi\uparrow}$, $\underline{L}_{\sigma\downarrow}$, and $\underline{L}_{\sigma\uparrow}$ ligand holes, respectively. Here, $\underline{L}_\sigma$ and $\underline{L}_\pi$ denote, respectively, e_g- and t_{2g}-symmetry combinations of holes on the ligand atoms. Charge-transfer states can mix with ionic states if they have the same symmetry. Thus we will have from just three basis states for the high spin d^8 configuration to a total of 36 basis states for the d^3 high spin configuration (see Table I).

The basis states were approximated by single Slater determinants, and only diagonal matrix elements were considered for the d-d Coulomb and exchange interactions in the model Hamiltonians. These matrix elements were expressed in terms of parameters $\mathcal{U}$, $\mathcal{U}'$, and $\mathcal{J}$. These parameters, originally proposed by Kanamori,[29] are $\mathcal{U} = \langle \xi\xi|H|\xi\xi\rangle$, the Coulomb interaction between d-

electrons in the same orbit; $u'=\langle \xi\eta|H|\xi\eta\rangle$, the Coulomb interaction between d electrons in different orbits; and $j=\langle \xi\eta|H|\eta\xi\rangle$, the exchange interaction ($\xi,\eta=3z^2-r^2$, x^2-y^2, xy, yz, or zx). u, u', and j are expressed in terms of A, B, and C Racah parameters in Table II. By using these parameters, the diagonal Coulomb-exchange-interaction energy for any configuration, $\varepsilon(d^{(n+m)}\underline{L}^m)$, is given relative to the center of gravity of the d^N multiplet by

$$\varepsilon(d^{(n+m)}\underline{L}^m) = [\tfrac{1}{2}N(N-1)-p]u'+pu - \tfrac{1}{2}[N_\uparrow(N_\uparrow-1)+N_\downarrow(N_\downarrow-1)]j-E(d^N) , \quad (3)$$

where $N=n+m=N_\uparrow+N_\downarrow$, the total number of $3d$ electrons for that configuration; $N_\uparrow$ and $N_\downarrow$ are the total number of spin-up and spin-down d electrons, respectively; p is the number of d-electron pairs in the same orbit; and $E(d^N)$ is the center of gravity of the d^N multiplet (see Table II). Electrostatic and orthogonalization contributions to the crystal-field splitting $10Dq$ have been found to be small (up to ≈ 0.5 eV) and were neglected for simplicity.[16]

The diagonal Hamiltonian matrix elements for the d^n-ion basis states are then

$$\langle d^n|H|d^n\rangle = 0 \quad \text{(reference)} ,$$

$$\langle d^{n+1}\underline{L}|H|d^{n+1}\underline{L}\rangle = \varepsilon(d^{n+1}\underline{L})-\varepsilon(d^n)+\Delta ,$$

$$\langle d^{n+2}\underline{L}^2|H|d^{n+2}\underline{L}^2\rangle = \varepsilon(d^{n+2}\underline{L}^2)-\varepsilon(d^n)+2\Delta+U ,$$

$$\vdots$$

$$\langle d^{n+m}\underline{L}^m|H|d^{n+m}\underline{L}^m\rangle = \varepsilon(d^{n+m}\underline{L}^m)-\varepsilon(d^n)+m\Delta+\tfrac{1}{2}m(m-1)U , \quad (4)$$

TABLE II. Basis functions, Hamiltonians, and parameters for the high-spin d^6 ($S=2$) and low-spin d^6 ($S=0$) configurations. Values for the B and C Racah parameters are listed in Table I. $E(d^N)$ is the center of gravity of the d^N multiplet, where N is the total number of $3d$ electrons for that configuration. $\Delta=E(d^{n+1}\underline{L})-E(d^n)$ is the ligand-to-metal charge-transfer energy, U is the on-site Coulomb repulsion energy; and u, u', and j are the Kanamori parameters.

High-spin d^6 ($^5T_2$) $S=2$		
$\phi_1=|t_{2\uparrow}^3 t_{2\downarrow} e_\uparrow^2\rangle$	$H_{1,1}=0$	
$\phi_2=|t_{2\uparrow}^3 t_{2\downarrow}^2 e_\uparrow^2 \underline{L}_{\pi\uparrow}\rangle$	$H_{2,2}=5u'+u-j-[E(d^7)-E(d^6)]+\Delta$	
$\phi_3=|t_{2\uparrow}^3 t_{2\downarrow} e_\uparrow^2 e_\downarrow \underline{L}_{\sigma\uparrow}\rangle$	$H_{3,3}=H_{2,2}$	
$\phi_4=|t_{2\uparrow}^3 t_{2\downarrow}^3 e_\uparrow^2 \underline{L}_{\pi\uparrow}^2\rangle$	$H_{4,4}=11u'+2u-3j-[E(d^8)-E(d^6)]+2\Delta+U$	
$\phi_5=|t_{2\uparrow}^3 t_{2\downarrow}^2 e_\uparrow^2 e_\downarrow \underline{L}_{\pi\uparrow}\underline{L}_{\sigma\uparrow}\rangle$	$H_{5,5}=H_{4,4}$	
$\phi_6=|t_{2\uparrow}^3 t_{2\downarrow} e_\uparrow^2 e_\downarrow^2 \underline{L}_{\sigma\uparrow}^2\rangle$	$H_{6,6}=H_{4,4}$	
$\phi_7=|t_{2\uparrow}^3 t_{2\downarrow}^3 e_\uparrow^2 e_\downarrow \underline{L}_{\pi\uparrow}^2 \underline{L}_{\sigma\uparrow}\rangle$	$H_{7,7}=18u'+3u-6j-[E(d^9)-E(d^6)]+3\Delta+3U$	
$\phi_8=|t_{2\uparrow}^3 t_{2\downarrow}^2 e_\uparrow^2 e_\downarrow^2 \underline{L}_{\pi\uparrow} \underline{L}_{\sigma\uparrow}^2\rangle$	$H_{8,8}=H_{7,7}$	
$\phi_9=|t_{2\uparrow}^3 t_{2\downarrow}^3 e_\uparrow^2 e_\downarrow^2 \underline{L}_{\pi\uparrow}^2 \underline{L}_{\sigma\uparrow}^2\rangle$	$H_{9,9}=26u'+4u-10j-[E(d^{10})-E(d^6)]+4\Delta+6U$	
$H_{1,2}=H_{2,4}=H_{3,5}=H_{5,7}=H_{6,8}=H_{8,9}=\sqrt{2}T_\pi$ $H_{1,3}=H_{2,5}=H_{3,6}=H_{4,7}=H_{5,8}=H_{7,9}=\sqrt{2}T_\sigma$		
Low-spin d^6 ($^1A_1$) $S=0$		
$\phi_1=|t_{2\uparrow}^3 t_{2\downarrow}^3\rangle$	$H_{1,1}=0$	
$\phi_2=|t_{2\uparrow}^3 t_{2\downarrow}^3 e_\uparrow \underline{L}_{\sigma\downarrow}\rangle$	$H_{2,2}=6u'-3j-[E(d^7)-E(d^6)]+\Delta$	
$\phi_3=|t_{2\uparrow}^3 t_{2\downarrow}^3 e_\downarrow \underline{L}_{\sigma\uparrow}\rangle$	$H_{3,3}=H_{2,2}$	
$\phi_4=|t_{2\uparrow}^3 t_{2\downarrow}^3 e_\uparrow^2 \underline{L}_{\sigma\downarrow}^2\rangle$	$H_{4,4}=13u'-7j-[E(d^8)-E(d^6)]+2\Delta+U$	
$\phi_5=|t_{2\uparrow}^3 t_{2\downarrow}^3 e_\uparrow e_\downarrow \underline{L}_{\sigma\downarrow}\underline{L}_{\sigma\uparrow}\rangle$	$H_{5,5}=12u'+u-6j-[E(d^8)-E(d^6)]+2\Delta+U$	
$\phi_6=|t_{2\uparrow}^3 t_{2\downarrow}^3 e_\downarrow^2 \underline{L}_{\sigma\uparrow}^2\rangle$	$H_{6,6}=H_{4,4}$	
$\phi_7=|t_{2\uparrow}^3 t_{2\downarrow}^3 e_\uparrow^2 e_\downarrow \underline{L}_{\sigma\downarrow}^2 \underline{L}_{\sigma\uparrow}\rangle$	$H_{7,7}=20u'+u-10j-[E(d^9)-E(d^6)]+3\Delta+3U$	
$\phi_8=|t_{2\uparrow}^3 t_{2\downarrow}^3 e_\uparrow e_\downarrow^2 \underline{L}_{\sigma\downarrow} L_{\sigma\uparrow}^2\rangle$	$H_{8,8}=H_{7,7}$	
$\phi_9=|t_{2\uparrow}^3 t_{2\downarrow}^3 e_\uparrow^2 e_\downarrow^2 \underline{L}_{\sigma\downarrow}^2 \underline{L}_{\sigma\uparrow}^2$	$H_{9,9}=28u'+2u-14j-[E(d^{10})-E(d^6)]+4\Delta+6U$	
$H_{1,2}=H_{1,3}=H_{2,4}=H_{2.5}=H_{3,5}=H_{3,6}=H_{4,7}$ $=H_{5,7}=H_{5,8}=H_{6,8}=H_{7,9}=H_{8,9}=\sqrt{2}T_\sigma$		
Parameters		
$T_\pi=2(pd\pi)$	$T_\sigma=\sqrt{3}(pd\sigma)$	For octahedral coordination
$T_\pi=(\frac{4}{3}(pd\sigma)^2+\frac{8}{9}(pd\pi)^2)^{1/2}$	$T_\sigma=2\sqrt{6}/3(pd\pi)$	For tetrahedral coordination
$T_\pi=0$	$T_\sigma=-[\frac{5}{12}(9(pd\sigma)^2+8(pd\pi)^2)]^{1/2}$	For pyrite-type compounds
$u=A+4B+3C$	$u'=A-B+C$	$j=\frac{5}{2}B+C$
$E(d^N)=\frac{1}{2}N(N+1)(A-\frac{14}{9}B+\frac{7}{9}C)=\frac{1}{2}N(N+1)U$		
$U=A-\frac{14}{9}B+\frac{21}{9}C$		

where Δ is the ligand-to-metal charge-transfer energy,

$$\Delta = E(d^{n+1}\underline{L}) - E(d^n) , \tag{5}$$

and U is the *d*-*d* Coulomb repulsion energy

$$U = E(d^{n-1}) + E(d^{n+1}) - 2E(d^n) . \tag{6}$$

Here, it should be noted that Δ and U are defined with respect to *the center of gravity of the multiplet of each configuration,* whereas they are defined with respect to the lowest level of the multiplet by Sawatzky and coworkers.[5,6] In the present paper, Δ and U defined in the latter way are referred to as Δ_{eff} and U_{eff} (see Table III). Racah parameters B and C for the TM cations were taken from Ref. 30 and are listed in Table I.

Hybridization between the ligand-*p* and metal-3*d* levels was included via the one-electron mixing matrix element T:

$$T = \langle d_\alpha | H | L_\alpha \rangle , \tag{7}$$

where d_α and L_α are a d electron and a ligand electron with the same orbital symmetry, respectively. We have included an anisotropic hybridization $T_\sigma \neq T_\pi$ to reflect the different transfer integrals for the ligand p_σ and p_π molecular orbitals. The off-diagonal Hamiltonian matrix elements are then

$$\begin{aligned}
&\langle (t_{2g\downarrow})_1^{n'} | H | (t_{2g\downarrow})^{n_1'+1} \underline{L}_{\pi\uparrow} \rangle = [(3-n_1')]^{1/2} T_\pi , \\
&\quad\vdots \\
&\langle (t_{2g\downarrow})^{n_1'+2} (\underline{L}_{\pi\uparrow})^2 | H | (t_{2g\downarrow})^{n_1'+3} (\underline{L}_{\pi\uparrow})^3 \rangle \\
&\qquad\qquad = [3(1-n_1')]^{1/2} T_\pi , \\
&\langle (e_{g\uparrow})^{n_2} | H | (e_{g\uparrow})^{n_2+1} \underline{L}_{\sigma\downarrow} \rangle = [(2-n_2)]^{1/2} T_\sigma , \\
&\langle (e_{g\uparrow})^{n_2+1} \vec{\underline{L}}_{\sigma\downarrow} | H | (e_{g\uparrow})^{n_2+2} (\underline{L}_{\sigma\downarrow})^2 \rangle = [2(1-n_2)]^{1/2} T_\sigma , \\
&\langle (e_{g\downarrow})^{n_2'} | H | (e_{g\downarrow})^{n_2'+1} \underline{L}_{\sigma\uparrow} \rangle = [(2-n_2')]^{1/2} T_\sigma , \\
&\langle (e_{g\downarrow})^{n_2'+1} \underline{L}_{\sigma\uparrow} | H | (e_{g\downarrow})^{n_2'+2} (\underline{L}_{\sigma\uparrow})^2 \rangle = [2(1-n_2')]^{1/2} T_\sigma ,
\end{aligned} \tag{8}$$

where n, n' and m, m' are defined as in Eq. (2). All other off-diagonal terms are zero. (No hybridization is considered for the $t_{2g\uparrow}$ electrons as they are totally filled for

TABLE III. Best-fit parameter values for Δ, U, and $(pd\sigma)$ (in eV), together with assignments for the main peaks and satellite structures, for various TM compounds. Values found in earlier configuration-interaction valence-band (Refs. 3, 4, 21, 23, and 24) and XAS (Ref. 17) studies are also included for comparison. For high-spin compounds, Δ and U values defined with respect to the lowest multiplet level of each configuration are given under Δ_{eff} and U_{eff}.

Compound	d^n	Valence	Δ	U	$(pd\sigma)$	Δ_{eff}	U_{eff}	Main peak	Satellite peak	Ref.
$SrMnO_3$	d^3	4+	2.0	7.8	−1.5	−0.2	7.1	$d^4\underline{L}$	$d^4\underline{L}$	This work
$LaMnO_3$	d^4	3+	4.5	7.5	−1.8	1.8	6.8	$d^5\underline{L}$	$d^6\underline{L}^2$	This work
MnO	d^5	2+	6.5	7.0	−1.1	8.8	11.6	$d^6\underline{L}$	d^5	This work
			7.0	7.5	−0.9					3
$Mn_{0.25}TiS_2$	d^5	2+	4.0	5.4	−0.9	6.3	10.0	$d^6\underline{L}$	d^5	This work
$Zn_{0.5}Mn_{0.5}s$	d^5	2+	4.0	5.8	−1.0	6.3	10.4	$d^6\underline{L}$	d^5	This work
$SrFeO_3$	d^4	4+	0.0	7.8	−1.3	−3.1	7.0	$d^5\underline{L}$	$d^6\underline{L}^2$	This work
$LaFeO_3$	d^5	3+	2.5	7.5	−1.4	5.3	13.6	$d^6\underline{L}$	d^5	This work
Fe_2O_3	d^5	3+	3.5	7.0	−1.4	6.3	12.7	$d^6\underline{L}$	d^5	This work
			3.0	8.0	−1.5					24
FeO	d^6	2+	6.0	7.0	−1.1	7.8	6.4	$d^7\underline{L}$	d^6	This work
			6.5	7.3	−1.0					23
$Fe_{0.33}TiS_2$	d^6	2+	3.5	5.5	−1.1	5.3	4.9	$d^7\underline{L}$	d^6	This work
FeS_2	d^6	2+	3.0	3.5	−0.8			$d^7\underline{L}$	d^6	This work
CoS_2	d^7	2+	2.5	4.2	−0.9			$d^8\underline{L}$	$d^9\underline{L}^2$	This work
NiO	d^8	2+	4.5	7.5	−1.3	5.2	6.8	$d^9\underline{L}$	$d^{10}\underline{L}^2$	This work
			4.0	7.5	−1.1					4
					−1.0	4.6	5.0			17
NiS	d^8	2+	2.5	5.5	−1.2	3.2	3.2	$d^9\underline{L}$	$d^{10}\underline{L}^2$	This work
			2.0	4.0	−1.5					21
$Ni_{0.33}TiS_2$	d^8	2+	2.5	6.0	−1.3	3.2	5.3	$d^9\underline{L}$	$d^{10}\underline{L}^2$	This work
NiS_2	d^8	2+	2.0	5.0	−1.1	2.7	4.3	$d^9\underline{L}$	$d^{10}\underline{L}^2$	This work
$NaCuO_2$	d^8	3+	−2.0	8.3	−1.6			$d^{10}\underline{L}^2$	$d^9\underline{L}$	This work
CuS	d^9	2+	0.5	7.0	−1.4			$d^{10}\underline{L}$	d^9	28

configurations greater than d^3 studied here.) For an octahedral coordination, $T_\sigma=\sqrt{3}(pd\sigma)$, $T_\pi=2(pd\pi)$, and we have assumed $(pd\sigma)/(pd\pi)\approx-2.2$, as in previous studies.[4] For the pyrite-type disulfides, T_π has been found to be very small from band-structure calculations,[31] although it does not enter the Hamiltonian matrix elements for the present cases. For these compounds we have assumed that

$$T_\sigma \approx -[\tfrac{5}{12}(9(pd\sigma)^2+8(pd\pi)^2)]^{1/2} \approx 2.1(pd\sigma)$$

(Ref. 32). For the tetrahedral case, we have set $T_\sigma=2\sqrt{6}/3(pd\pi)$ and

$$T_\pi=[(2\sqrt{3}/3(pd\sigma))^2+(2\sqrt{2}/3(pd\pi))^2]^{1/2} .$$

The eigenfunctions for the ground state are found by diagonalization of the Hamiltonian matrix. Examples of basis states and Hamiltonians found for the high-spin d^6 ($S=2$) and low-spin d^6 ($S=0$) configurations by this model, together with the various parameters used, are detailed in Table II.

The XPS final states will differ from the ground state by the attraction between the photoionization core hole and the $3d$ electron Q, which pulls down the $3d$ levels. If we take the same basis set as was used for the ground state, but with the presence of a core hole $\underline{c}$, then the diagonal matrix elements are

$$\langle \underline{c}d^n|H|\underline{c}d^n\rangle = E_c ,$$

$$\langle \underline{c}d^{n+1}\underline{L}|H|\underline{c}d^{n+1}\underline{L}\rangle = E_c+\varepsilon(d^{n+1}\underline{L})-\varepsilon(d^n)+\Delta-Q ,$$

$$\langle \underline{c}d^{n+2}\underline{L}^2|H|\underline{c}d^{n+2}\underline{L}^2\rangle$$
$$= E_c+\varepsilon(d^{n+2}\underline{L}^2)-\varepsilon(d^n)+2(\Delta-Q)+U ,$$
$$\vdots$$
$$\langle \underline{c}d^{n+m}\underline{L}^m|H|\underline{c}d^{n+m}\underline{L}^m\rangle$$
$$= E_c+\varepsilon(d^{n+m}\underline{L}^m)-\varepsilon(d^n)$$
$$+m(\Delta-Q)+\tfrac{1}{2}m(m-1)U , \tag{9}$$

where E_c is the core-hole energy relative to the ionic lattice. We have neglected the exchange interaction between the core hole and the d electrons and have assumed the relationship $U/Q\approx0.83$ as before.[25] Note, however, that $U/Q\approx0.8$ is not a unique choice: If we use $U/Q\approx0.7$ as in other studies,[15,16] the estimated U values correspondingly become smaller by $\sim15\%$. In this sense, the U values obtained here may not have absolute meaning.

After finding the eigenfunctions of the final-state matrix, the XPS spectrum $\rho(e_k)$ is given in the sudden approximation by

$$\rho(e_k)=\sum_f |\langle\Psi_f|c|\Psi_g\rangle|^2\delta(h\nu-e_k-E_f) , \tag{10}$$

where c is the annihilation operator of the core electron and the right-hand side is summed over all final states. Here, Ψ_f and Ψ_g are the wave functions of the final and initial states, respectively; E_f are the final-state energies; $h\nu$ the photon energy; and e_k the kinetic energy of the photoelectron. By using Eq. (10) and having a knowledge about the three adjustable parameters Δ, U, and $(pd\sigma)$, we can calculate the cluster-approximation prediction for the energy separations and intensities of the core-level XPS spectral features. It was found that the inclusion of the d-d exchange interaction and the anisotropic hybridization were essential in reproducing the experimental spectra using reasonable parameter values.

IV. RESULTS AND DISCUSSION

Using the above model, we have obtained calculated $2p$ core-level XPS spectra for the TM compounds by varying the parameters Δ, U, and $(pd\sigma)$ to provide a best fit to the experimental data. Excellent agreement was consistently found between theory and experiment. Each spectrum consists of a main spin-orbit doublet accompanied by higher-energy states which comprise the satellite structure. A Lorentzian lifetime broadening $\Gamma_0=0.8-1.6$ eV was used to match the main peaks to the experimental data. For higher-energy states, a virtual-bound-state-type broadening[33] was also included to simulate the greater lifetime broadening of the higher-energy states, as well as the core-hole–d-electron multiplet splitting, the effect of the finite ligand widths, and additional splitting due to the off-diagonal d-d Coulomb exchange interactions neglected in the present Hamiltonians. Such

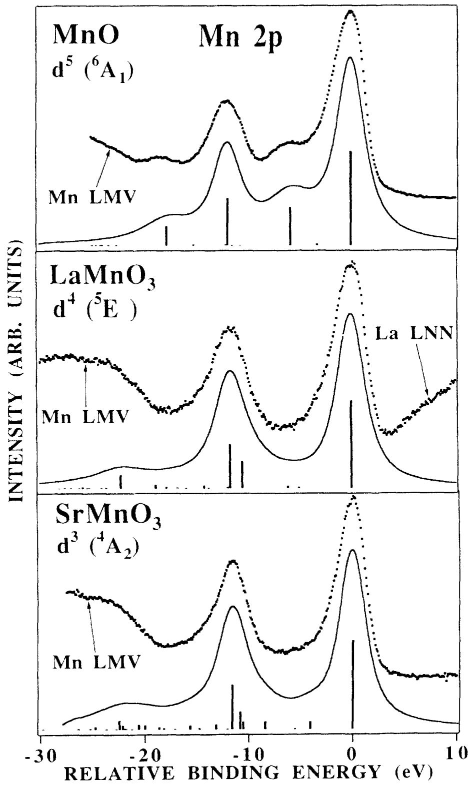

FIG. 1. Theoretical $2p$ core-level XPS spectra (solid line) compared with experimental data (dots) after background subtraction for Mn cations with varying valence. Emission due to the Mn LMV Auger peak is observed on the high-binding-energy side of the $2p_{1/2}$ spin-orbit peak, partially obscuring the $2p_{1/2}$ satellite structure.

broadening has also been used to describe the $4f$ spectra of rare-earth compounds.[33] Thus, the satellite peaks were broadened by an additional factor proportional to their energy separation from the main peak ΔE, such that the Lorentzian full width at half maximum (FWHM) is

$$2\Gamma_n = 2\Gamma_0(1+\alpha\Delta E) , \tag{11}$$

where Γ_n is the lifetime broadening of the satellite peak and α is a constant. Values for the product $\Gamma_0\alpha$ were kept in the range 0.07–0.25. (For FeS_2 and CoS_2, which show narrow main peaks and broad satellites, $\Gamma_0\alpha \approx 0.3$ with small Γ_0 had to be employed.) A Gaussian broadening of 1.4 eV FWHM was also used for the entire spectrum to simulate the instrumental resolution and other broadening effects.

Calculated spectra are compared to experimental data in Figs. 1–7. All spectra display a spin-orbit doublet split into $2p_{3/2}$ and $2p_{1/2}$ peaks located at lower and higher binding energies, respectively. They have been aligned to the binding energies of the $2p_{3/2}$ main peaks, and only relative binding energies are considered here. Satellites for the $2p_{1/2}$ spin-orbit doublet were not seriously considered in the fitting procedure due to the appearance in this region of bulk-plasmon satellites accompanying the $2p_{3/2}$ main peak. (Fe $2p$ and Mn $2p$ core-level spectra collected with Mg $K\alpha$ x rays will also exhibit intensity in this region which partially obscures the $2p_{1/2}$ satellite due to O *KLL* and Mn *LMV* auger emission, respectively.) Further, the shape of the $2p_{1/2}$ satellite structure can differ considerably from that of the $2p_{3/2}$ structure due to strong interference effects in the $2p_{1/2}$ spectrum resulting from a Coster-Kronig decay.[34]

Strong satellite structures are observed for most of the oxides and sulfides, with less distinct structures found for some sulfides and perovskite-type oxides. Spectra for the low-spin disulfides showed apparently very weak satellite structure. For spectra of metallic or semimetallic (NiS, M_xTiS_2, CoS_2, and $SrFeO_3$) and narrow-gap semiconducting (FeS_2, NiS_2, and $LaMnO_3$) compounds, the asymmetric nature of the main peaks leads to small discrepancies on the high-binding-energy side of these peaks when compared to the calculated spectra. Model parameter values were varied to match the shape, intensity, and position of the satellite features, meaning that spectra with

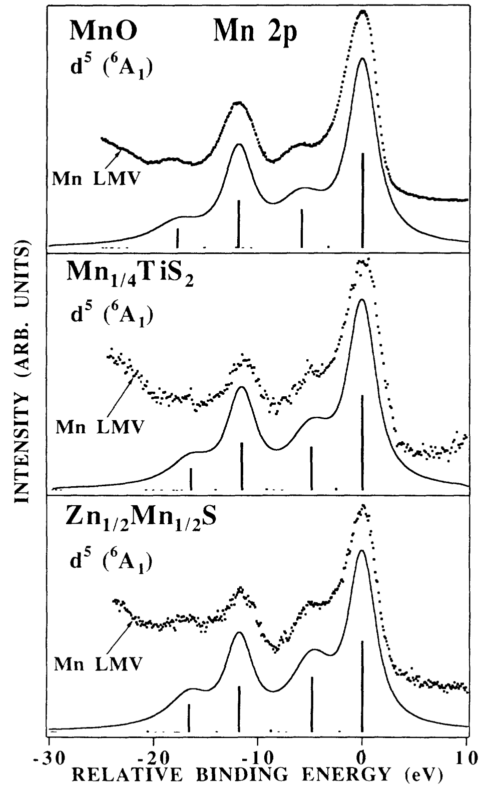

FIG. 2. Theoretical $2p$ core-level XPS spectra (solid line) compared with experimental data (dots) after background subtraction for Mn cations with varying ligands. Emission due to the Mn *LMV* Auger peak is observed on the high-binding-energy side of the $2p_{1/2}$ spin-orbit peak, partially obscuring the $2p_{1/2}$ satellite structure. The experimental data for $Mn_{0.25}TiS_2$ are taken from Ref. 18.

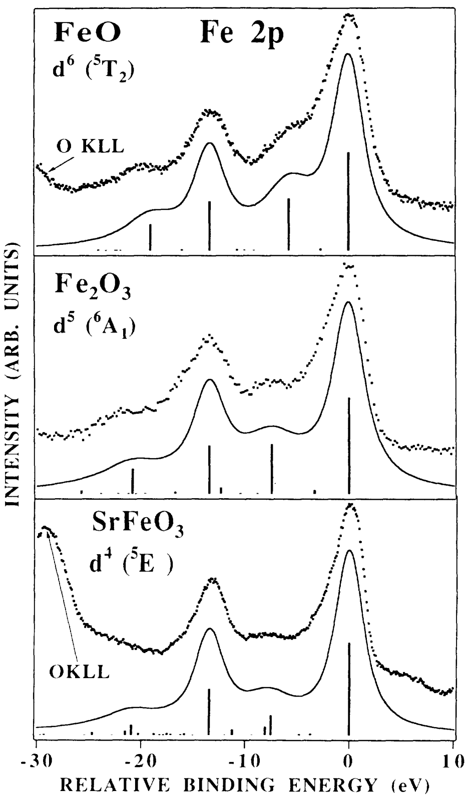

FIG. 3. Theoretical $2p$ core-level XPS spectra (solid line) compared with experimental data (dots) after background subtraction for Fe cations with varying valence. Data for $LaFeO_3$ are similar to those for Fe_2O_3. Emission due to the O *KLL* Auger peak is observed on the high-binding-energy side of the $2p_{1/2}$ spin-orbit peak for FeO and $SrFeO_3$, partially obscuring the $2p_{1/2}$ satellite structure. The spectrum for Fe_2O_3 was collected using an Al $K\alpha$ source and does not show this structure. The experimental data for Fe_2O_3 and $SrFeO_3$ are taken from Refs. 24 and 25, respectively.

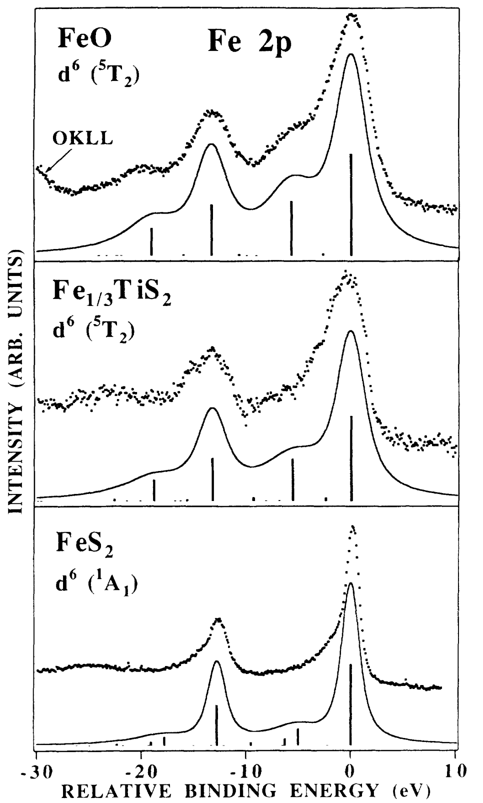

FIG. 4. Theoretical 2p core-level XPS spectra (solid line) compared with experimental data (dots) after background subtraction for Fe cations with varying ligands. For the FeO spectrum, emission due to the O *KLL* Auger peak is observed on the high-binding-energy side of the $2p_{1/2}$ spin-orbit peak, partially obscuring the $2p_{1/2}$ spin-orbit peak, partially obscuring the $2p_{1/2}$ satellite structure. Bulk-plasmon satellites accompanying the main peak are also observed for both sulfide spectra at ≈ 25 eV. The experimental data for $Fe_{0.33}TiS_2$ are taken from Ref. 18.

distinct satellites would be more successfully modeled.

Errors bars were in the range ± 0.5 eV for Δ and U, and ± 0.05–0.1 eV for $(pd\sigma)$ when they are varied independently. It is difficult to define error bars uniquely, however, since these parameters are correlated with each other. For example, error bars for Δ and U amount to ± 1 eV when they are varied with $\Delta - U$ kept constant. Error bars are larger for spectra with weak satellites such as those of pyrite-type compounds, $SeFeO_3$, and Mn perovskites. Best-fit values for Δ, U, and $(pd\sigma)$, together with values for Δ_{eff} and U_{eff} calculated within Kanamori's parametrization, are listed in Table III.

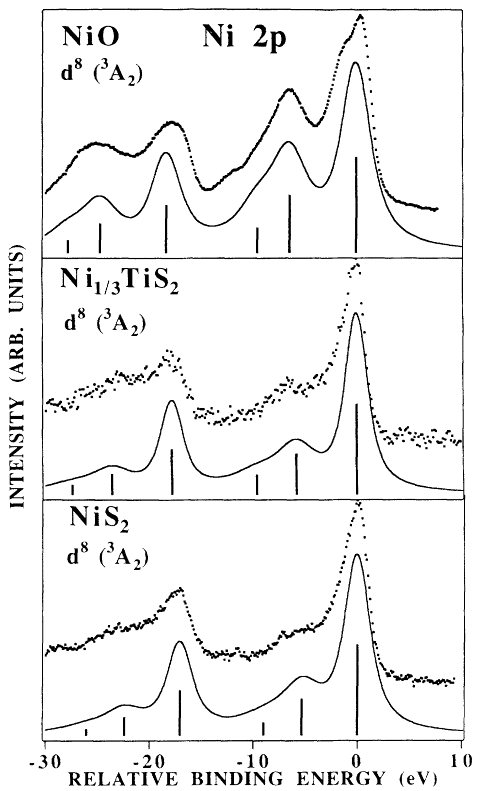

FIG. 6. Theoretical 2p core-level XPS spectra (solid line) compared with experimental data (dots) after background subtraction for Ni cations with varying ligands. Bulk-plasmon satellites accompanying the main peak are observed for all spectra at ≈ 25 eV. The experimental data for $Ni_{0.33}TiS_2$ are taken from Ref. 18.

A comparison of parameter values found from the

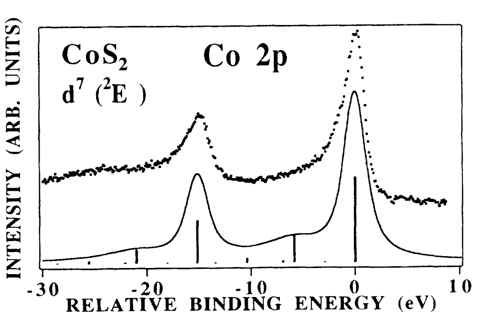

FIG. 5. Theoretical 2p core-level XPS spectrum (solid line) compared with experimental data (dots) after background subtraction for CoS_2. A bulk-plasmon satellite accompanying the main peak is observed at ≈ 25 eV.

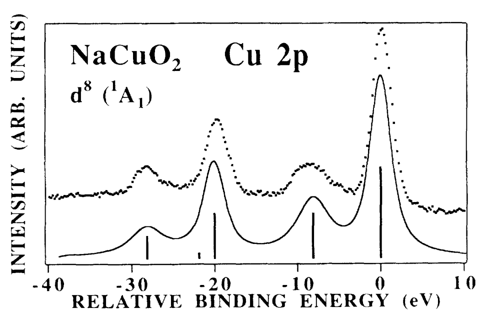

FIG. 7. Theoretical 2p core-level XPS spectrum (solid line) compared with experimental data (dots) after background subtraction for $NaCuO_2$. The experimental data for $NaCuO_2$ are taken from Ref. 22.

core-level XPS spectra with those found previously from configuration-interaction valence-band and core-level XAS studies (also listed in Table III), in which Coulomb exchange interaction and anisotropic hybridization have been fully taken into account, reveals a remarkable consistency. The success of this model to reproduce the core-level spectra using parameter values found for the valence band gives us confidence that it can be used indirectly to determine the valence-electronic structure of the TM compounds.

A. Systematics of the electronic structures

The values for U, Δ, and $(pd\sigma)$ listed in Table III are displayed graphically in Figs. 8–10 with respect to changes in the cation atomic number, ligand electronegativity, and cation valence. We also include here values found in previous studies of compounds not covered by this work. The values of Δ and U follow consistent chemical trends that can be well understood, and reflect those found earlier by Zaanen and Sawatzky.[1]

Within any series of compounds with the same ligand, it is seen that Δ decreases in going from the left to the right of the TM series (Mn→Cu), as expected. This reflects the increase in electronegativity of the metal cation or the lowering of the metal $3d$ orbitals with atomic number, as found by many first-principles cluster[19] and band-structure calculations.[35] With respect to U, there will be an overall increase along the same direction because of the decrease in the radial extent of the $3d$ orbitals.

For compounds with the same cation, an increase in ligand electronegativity will lower the ligand p bands with respect to the metal d orbitals, resulting in an increase in Δ. This has been shown to be the case for Ni, where band calculations predict the ligand p bands to be at lower energies for NiO (Ref. 36) than for NiS.[37] This trend is observed for all cations, with Δ decreasing as we go from the highly electronegative O^{2-} ligands to the less electronegative S^{2-} or S_2^{2-} ligands, confirming a trend found previously for the dihalide compounds, $M\mathrm{Cl}_2$, $M\mathrm{Br}_2$, and $M\mathrm{I}_2$.[13,15,16] U is also seen to decrease along the series $MO \rightarrow M_x\mathrm{TiS}_2$, $MS \rightarrow MS_2$, probably due to the increased polarizability of the ligand species, which screens the electrostatic potential U. This polarizability will be particularly large for the pyrite-type compounds, where the S $3p$ orbitals are only partially occupied, leading to small values of U for these compounds.

Trends for compounds with the same cation, but with increasing metal ion valence, will be governed by the decrease in the number of d electrons present. As the ionic charge increases, the $3d$ orbitals are lowered, leading to a decrease in the magnitude of Δ. This trend is clearly seen for the Fe and Mn oxides. For Cu oxides, also, $\Delta \approx 2$ eV for $\mathrm{Cu}^{2+}\mathrm{O}$,[6,38] and $\Delta \approx -2$ eV for $\mathrm{NaCu}^{3+}\mathrm{O}_2$. As the number of d electrons falls, we would also expect an increase in U, due to the shrinking radius of the $3d$ orbitals. Such a trend is only weakly observed in the data.

Trends for the overlap integral will be primarily governed by the interatomic distances within the cluster, largely determined by the ionic radii of the metal and ligand ions. As the interatomic distance decreases, greater overlap of the $3d$ orbitals with the p bands increases the value of $(pd\sigma)$. As can be seen in Fig. 10 and Table III, however, trends for $(pd\sigma)$ are not so outstanding as those for Δ and U. Zaanen and Sawatzky[1] have ar-

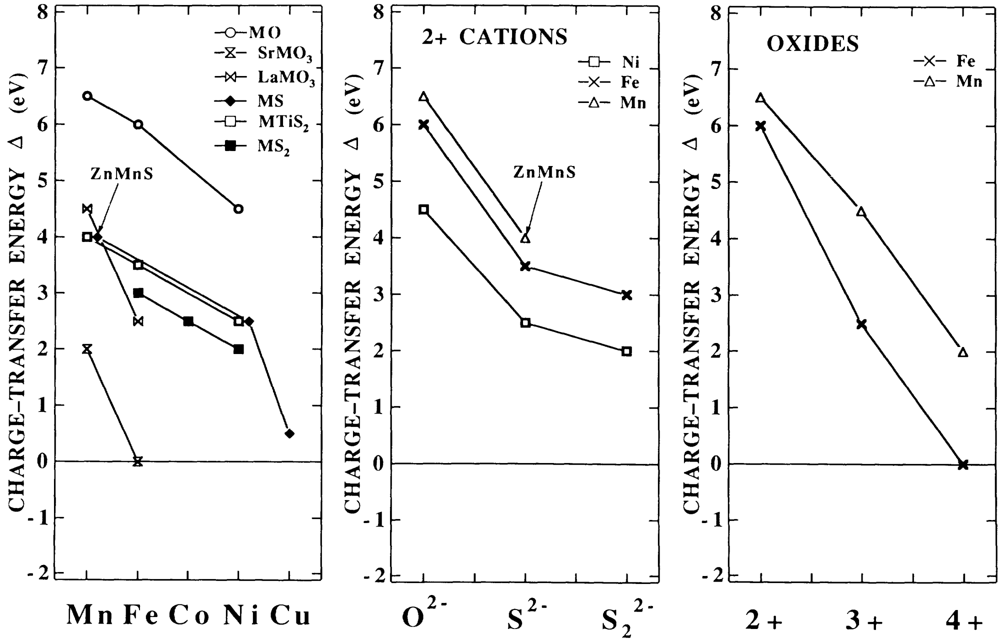

FIG. 8. Charge-transfer energies Δ for the transition-metal compounds displayed with respect to cation atomic number, ligand electronegativity, and cation valence.

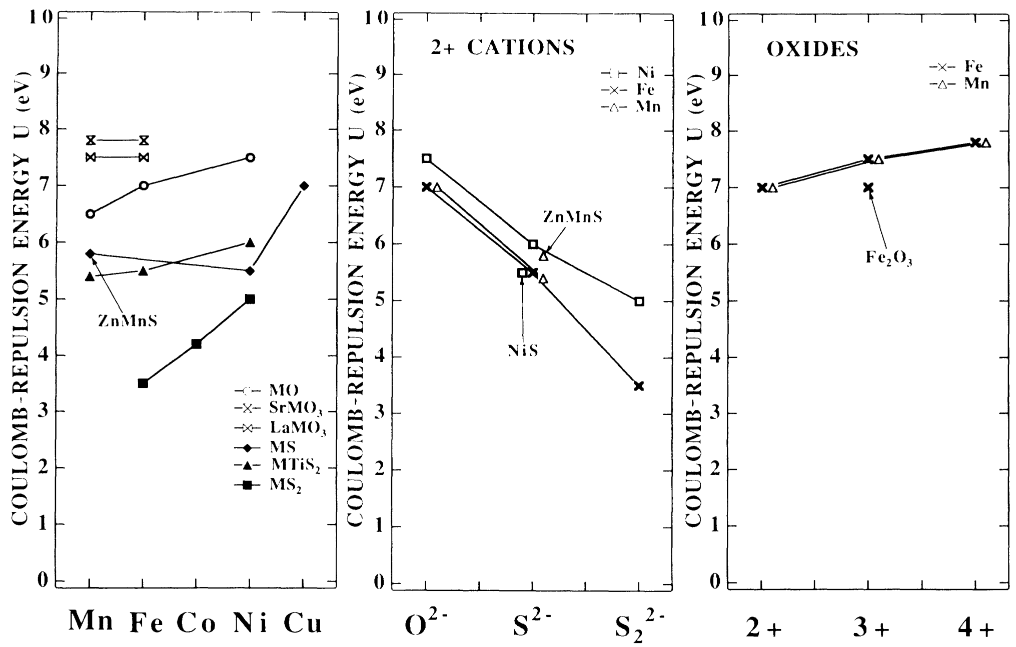

FIG. 9. On-site *d-d* Coulomb repulsion energies U for the transition-metal compounds displayed with respect to cation atomic number, ligand electronegativity, and cation valence.

gued that T_σ and T_π do not vary much over various compounds, since the interatomic distances are determined by the balance between chemical bond formation and repulsion between the ion cores. Further, Zaanen, Westra, and Sawatzky[15] have pointed out that T_σ and T_π, which were assumed constant in Eq. (8) for all off-diagonal terms, will vary depending on the number of screening electrons in the presence of a core hole. Thus, taking into account the uncertainty in this parameter, the values for $(pd\sigma)$ in Table III and Fig. 10 should be interpreted with caution.

Nevertheless, the following gross general trends may

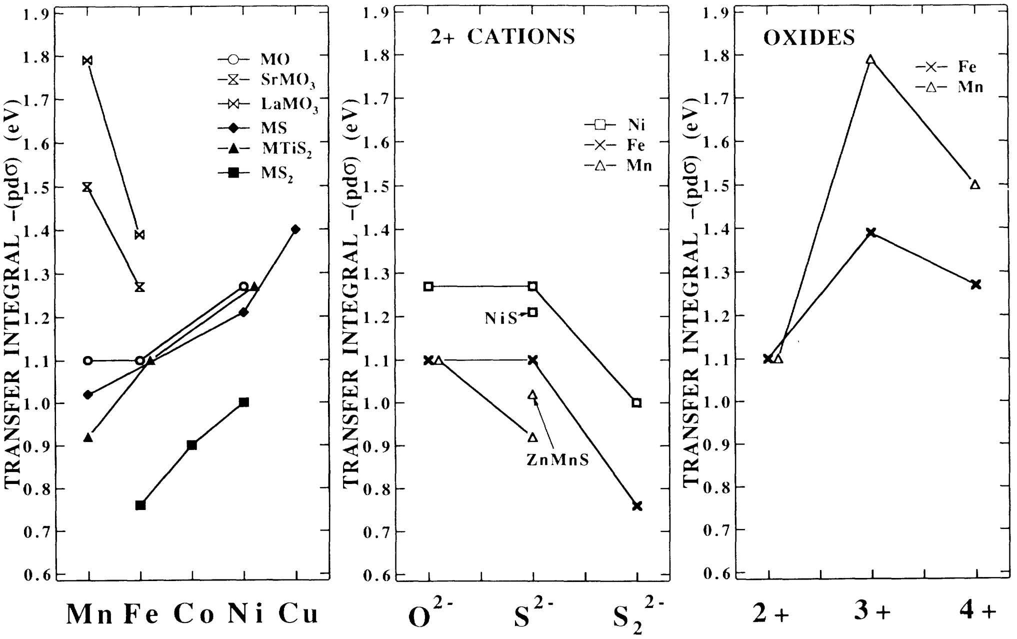

FIG. 10. Ligand-p-metal-d transfer integrals $(pd\sigma)$ of the e_g and p_σ orbitals for the transition-metal compounds displayed with respect to cation atomic number, ligand electronegativity, and cation valence.

be noted for $(pd\sigma)$. As we go from Fe to Cu, $(pd\sigma)$ is seen to increase, reflecting the smaller ionic radii of the cations and, hence, smaller bond lengths of the heavier cations. It was also found that $(pd\sigma)$ increases when going from Fe to Mn. This could be largely attributed to the contraction of the metal-ligand bond length as the strongly antibonding e_g orbitals are progressively emptied. For the series $MO \rightarrow M_x\mathrm{TiS}_2 \rightarrow M\mathrm{S}_2$, we note a general decrease in $(pd\sigma)$ as the ligand changes. This reflects the fact that the metal-sulfur distances are larger in the intercalation compounds than in the metal-oxygen distances in the oxides, and the even larger interatomic metal-sulfur distances found in the pyrite-type compounds.[20,31] For $\mathrm{Zn_{0.5}Mn_{0.5}S}$, we find $(pd\sigma)$ larger than that of $\mathrm{Mn_{0.25}TiS_2}$, reflecting the smaller bond length for the tetrahedral coordination. It is interesting to note that, apart from the larger $(pd\sigma)$ arising from the shorter Mn-S distance, Δ and U for $\mathrm{Zn_{0.5}Mn_{0.5}S}$ are nearly the same as those for $\mathrm{Mn_{0.25}TiS_2}$, in spite of the different S coordinations. It should also be noted here that predictions for $(pd\sigma)$ of the disulfide compounds using this model may be somewhat inaccurate as we have not included transfer with empty S $3p$ orbitals, i.e., the σ^* antibonding orbitals of the S_2^{2-} molecule. Finally, we see $(pd\sigma)$ increases from a divalent to a trivalent state, again reflecting the shrinking size of the cation as the ionic charge increases. However, $(pd\sigma)$ decreases back from the trivalent to a tetravelent state ($\mathrm{SrFeO_3}$ and $\mathrm{SrMnO_3}$), but we should note that the weak satellites in the latter compounds preclude accurate determination of the parameters.

Having gained some confidence in our predictions of Δ and U, we can construct a Zaanen-Sawatzky-Allen[1] (ZSA) Δ-U diagram as shown in Fig. 11. For $U > \Delta$, the band gaps of the TM compounds will be of a charge-transfer type determined by the magnitude of Δ. Metallic compounds with small or negative Δ can be classified as p-type metals with holes in the ligand p bands strongly mixed with metal d states,[28] and for insulating compounds with negative Δ, we will have a p-p band gap related to neither Δ nor U.[22] This small or negative Δ region in the phase diagram can be dubbed the "valence bond regime" to distinguish between the local intracluster hybridization and the extended intercluster hybridization processes which stabilize and destabilize the insulating state, respectively.[22] For $U < \Delta$, we are in the Mott-Hubbard regime, with band gaps of a d-d type, where compounds with a small U will be d-band metals in the traditional sense. It is now well accepted that the early-TM compounds fall in the Mott-Hubbard regime. In Fig. 11 we have separated the divalent TM compounds from the trivalent and tetravalent compounds for clarity.

Most of the TM compounds studied in this work are classified in the charge-transfer regime of the diagram, with $\mathrm{NaCuO_2}$ falling in the negative-Δ regime. Several compounds, including the Fe and Mn monoxides and sulfides fall near the boundary with the Mott-Hubbard regime. $\mathrm{CoS_2}$ and $\mathrm{FeS_2}$ also fall near the boundary, due to the small U's deduced for these compounds from the present analysis. It should be noted, however, that parameters for these compounds are not so definite due to their indistinct satellite structures and the approximate treatment of the unoccupied ligand p orbitals, as noted above. All the higher valence compounds studied fall in the charge-transfer regime. Chemical trends for Δ and U noted above can also be observed in this diagram. This picture confirms the growing consensus[1,15,16] that for late-TM compounds, the basic Mott-Hubbard description of the charge fluctuations breaks down and that charge-transfer interactions are central to understanding the electronic structure of these compounds.

For $\mathrm{CoS_2}$ and $\mathrm{FeS_2}$, it would be interesting to see whether the d-d Coulomb interactions are small enough that these compounds are well described using a simple one-electron band picture, instead of the local-cluster approach.[20,39] The unusually large values of $(pd\sigma)$ for $\mathrm{LaMnO_3}$ and $\mathrm{SrMnO_3}$ deduced here might also indicate a limitation of the local-cluster approach, since a large value for T, combined with the large number of empty $3d$

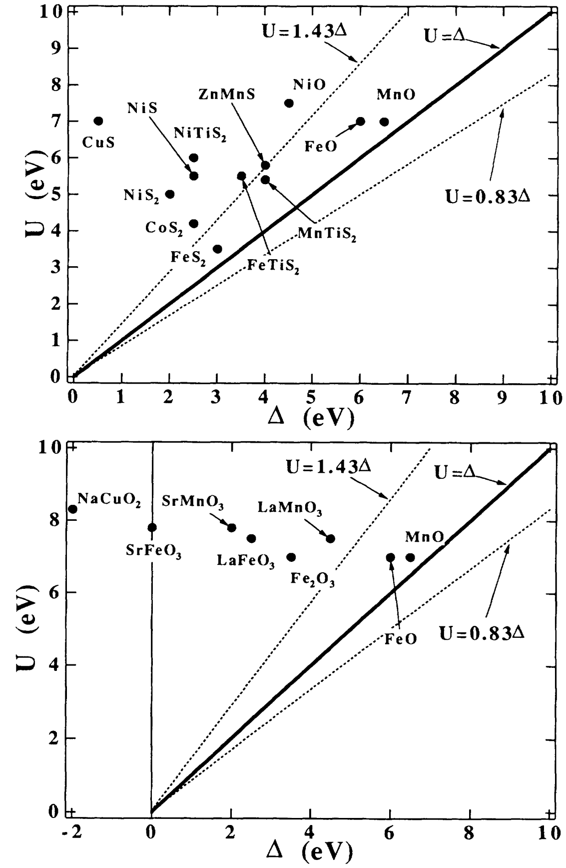

FIG. 11. Zaanen-Sawatzky-Allen Δ-U diagram indicating the positions of the divalent (top) and higher valent (bottom) transition-metal compounds studied in this work (circles). The region above the line $U=\Delta$ is the charge-transfer regime, in which the transition-metal compounds will have a charge-transfer band gap determined by the magnitude of Δ. The region below this line is the Mott-Hubbard regime, where the band gaps will be of a d-d type. For the lines $U=1.43\Delta$ and $U=0.83\Delta$, see text.

states, will inevitably lead to strong hybridization between neighboring clusters mediated by the intervening oxygen orbitals. The applicability of the cluster model to TM systems with smaller d-electron numbers (d^3, d^2, etc.) thus remains to be further investigated, particularly in relation to the exciton satellite mechanism proposed earlier for the early-TM compounds.[40]

Apart from the limitations of the local-cluster approach itself, there are some effects that are not explicitly included in our model but are considered through the phenomenological linewidth broadening, namely, effects of the core-hole–d-electron multiplet coupling and the off-diagonal d-d Coulomb exchange interactions. Recently, Okada, Kotani, and Thole[41,42] have calculated the $2p$ and $3s$ core-level XPS spectra of Ni^{2+} and Co^{2+} dihalides including these effects, i.e., the full multiplet effect, and obtained parameters consistent with those deduced from valence-band studies. This result would justify our model in which only the diagonal d-d Coulomb exchange interaction has been incorporated. Such a justification remains to be done for lighter TM compounds, but similar full-multiplet cluster-model calculations for these compounds would require considerably more computational effort.

B. Spectral assignment

The main peaks and satellite structures for the TM compounds with d^n ground states can primarily be assigned to $|\underline{c}d^n\rangle$, $|\underline{c}d^{n+1}\underline{L}\rangle$, and $|\underline{c}d^{n+2}\underline{L}^2\rangle$ final states. Other configurations appear with negligible intensity at higher energies. These assignments are listed in detail in Table III. For compounds falling within the charge-transfer regime, the screening process in the XPS final state will mean that the lowest-energy configuration is that of a well-screened state. We can now distinguish various regions within this regime as a function of Δ. For compounds with moderate covalency, $Q-U<\Delta<Q-\frac{1}{2}U$ [i.e., $\Delta-Q<0$, $2\Delta+U-2Q<0$, and $2\Delta+U-2Q>\Delta-Q$; see Eq. (9)], the lowest-energy configuration will be that of a $|\underline{c}d^{n+1}\underline{L}\rangle$ final state and the main peaks of these compounds can be assigned to those states. The next lowest-energy configuration will be due to $|\underline{c}d^{n+2}\underline{L}^2\rangle$ final states, while the $|\underline{c}d^n\rangle$ state lies at higher energy still, although the satellite intensity is still borrowed from this component. Thus, satellites for the compounds lying above the line $U\approx1.43\Delta$ in Fig. 11,

$$\Delta<Q-\tfrac{1}{2}U\approx1.2U-0.5U=0.7U\ ,$$

will have satellites primarily due to a $|\underline{c}d^{n+2}\underline{L}^2\rangle$ final state. This agrees with trends found earlier for $NiCl_2$ and $NiBr_2$.[15]

For strongly covalent compounds, such as $NaCuO_2$, where $\Delta<Q-U$, the $|\underline{c}d^{n+2}\underline{L}^2\rangle$ final state will now be the lowest in energy and the satellite will be due to a $|\underline{c}d^{n+1}\underline{L}\rangle$ final state. Finally, we have an intermediate region for moderately ionic compounds where $Q-\frac{1}{2}U<\Delta<Q$ (compounds lying between the $U\approx0.83\Delta$ and $U\approx1.43\Delta$ lines in Fig. 11). Here, the main peak should still be due to screened $|\underline{c}d^{n+1}\underline{L}\rangle$ final states, and the satellite should appear with mainly poorly screened $|\underline{c}d^n\rangle$ final-state character. For MnO, although it is categorized in this region, screening plays a less prominent role in the XPS final state, and the main peaks are found to be due to the unscreened $|\underline{c}d^n\rangle$ final states, with the satellites arising from the $|\underline{c}d^{n+1}\underline{L}\rangle$ final states, i.e., the satellite originates from a shakeup transition. This can be attributed to the strong exchange stabilization of the half-filled d^5 shell in the XPS final states, i.e., the Δ_{eff} value considerably larger than Δ as shown in Table III.

V. CONCLUSIONS

We have extended the charge-transfer configuration-interaction model proposed by van der Laan *et al.*[13] and Zaanen, Westra, and Sawatzky[15] to investigate the electronic structures of a wide range of TM compounds. We find that by including in the model Hamiltonians the exchange interaction and an anisotropic hybridization effect,[43] we can successfully reproduce the $2p$ core-level XPS spectra of compounds ranging from d^3 $SrMnO_3$ to d^8 NiO and $NaCuO_2$. Parameter values found from analysis of the core levels compare well with those obtained earlier in various, more elaborate valence-band configuration-interaction studies, giving us confidence that this model can indirectly predict the valence-electronic structures of the TM compounds.

Trends for the parameters Δ and U are easily understood and follow expected chemical tendencies, as are those for $(pd\sigma)$ to some extent. By using these values of Δ and U, we have constructed a ZSA-type Δ-U diagram, in which most of the late-TM compounds studied in this work have been classified as charge-transfer insulators or a charge-transfer metal. We find that for all compounds in the charge-transfer regime with positive Δ, the main peak corresponds to screened $|\underline{c}d^{n+1}\underline{L}\rangle$ final states, while the assignment of the satellite peak varies between the $|\underline{c}d^{n+2}\underline{L}^2\rangle$ and $|\underline{c}d^n\underline{L}\rangle$ final states, depending on the ionicity of the compound. This picture confirms the growing consensus that for the late-TM compounds, charge-transfer interactions are central to understanding the electronic structure of these compounds and that a many-body configuration-interaction approach is necessary in order to understand the core-level spectra.

Some important aspects, however, have not yet been clarified in the present work. These include the effects of unoccupied ligand orbitals in the pyrite-type disulfides on the cluster-model analysis. The applicability of the cluster model to TM systems with smaller d-electron numbers (d^3, d^2, etc.) also remains to be examined in future studies. For a more complete understanding of the spectra of the TM compounds, more elaborate calculations which include the multiplet coupling between the core hole and d electrons would be desirable. However, from a practical point of view, the success of the present simple model indicates that core-level photoemission spectroscopy is a promising diagnostic tool to study the valence-electronic structure of more complicated materials, such as impurity systems, for which it is difficult to deduce *d*-derived features in the valence-band spectra.

ACKNOWLEDGMENTS

The authors would like to thank Professor J. C. Fuggle for valuable discussions. We also thank Professor S. Suga for taking Al $K\alpha$ spectra and providing the FeS_2 sample, and Dr. N. Kimizuka (FeO), Dr. M. Saeki (Fe_2O_3), Professor N. Mori (NiS_2), Professor T. Miyadai (CoS_2), Dr. S. Kimura (MnO), Dr. T. Chiba (NiO), Professor Y. Takeda and Professor M. Takano ($LaMnO_3$ and $SrMnO_3$), Professor S. Anzai and Dr. M. Matoba (NiS), and Professor S. Nakashima ($Zn_{0.5}Mn_{0.5}S$), for the supply of samples. This work is supported by a Grant-in-Aid for Scientific Research from the Ministry of Education, Science and Culture (Monbusho) and Toray Science Foundation. One of us (A.E.B.) gratefully acknowledges partial support also by Monbusho.

---

*Present address: Department of Physics, La Trobe University, Bundoora, VIC 3083, Australia.

†Author to whom correspondence should be addressed.

[1] J. Zaanen, G. A. Sawatzky, and J. W. Allen, Phys. Rev. Lett. **55**, 418 (1985); J. Zaanen and G. A. Swawatzy, Can J. Phys. **65**, 1262 (1987); J. Solid State Chem. **88**, 8 (1990).

[2] See, e.g., W. E. Pickett, Rev. Mod. Phys. **61**, 443 (1989).

[3] A. Fujimori, N. Kimizuka, T. Akahane, T. Chiba, S. Kimura, F. Minami, K. Siratori, M. Taniguchi, S. Ogawa, and S. Suga, Phys. Rev. B **42**, 7580 (1990).

[4] A. Fujimori and F. Minami, Phys. Rev. B **30**, 957 (1984).

[5] J. van Elp, J. L. Wieland, H. Eskes, P. Kuiper, G. A. Sawatzky, F. M. F. de Groot, and J. S. Turner, Phys. Rev. B **44**, 6090 (1991).

[6] J. Ghijsen, L. H. Tjeng, H. Eskes, G. A. Sawatzky, and R. L. Johnson, Phys. Rev. B **42**, 2268 (1990); H. Eskes, L. H. Tjeng, and G. A. Sawatzky, *ibid.* **41**, 288 (1990).

[7] See, e.g., G. Wendin, Struct. Bonding (Berlin) **45**, 1 (1981).

[8] See, e.g., A. Fujimori, Phys. Rev. B **28**, 2281 (1983); A. Kotani, T. Jo, and J. C. Parlebas, Adv. Phys. **37**, 37 (1988).

[9] R. P. Gupta and S. K. Sen, Phys. Rev. B **12**, 15 (1975).

[10] A. Rosencwaig, G. K. Wertheim, and H. J. Guggenheim, Phys. Rev. Lett. **27**, 479 (1971).

[11] K. S. Kim, J. Electron Spectrosc. Relat. Phenom. **3**, 217 (1974).

[12] B. W. Veal and A. P. Paulikas, Phys. Rev. B **31**, 5399 (1985); B. W. Veal, D. E. Ellis, and D. J. Lam, *ibid.* **32**, 5391 (1985).

[13] G. van der Laan, C. Westra, C. Haas, and G. A. Sawatzky, Phys. Rev. B **23**, 4369 (1981).

[14] S. Larsson, Chem. Phys. Lett. **32**, 401 (1975); **40**, 362 (1976); S. Larsson and M. Braga, *ibid.* **48**, 596 (1977).

[15] J. Zaanen, C. Westra, and G. A. Sawatzky, Phys. Rev. B **33**, 8060 (1986).

[16] J. Park, S. Ryu, M.-S. Han, and S.-J. Oh, Phys. Rev. B **37**, 10 867 (1988).

[17] G. van der Laan, J. Zaanen, G. A. Sawatzky, R. Kartanak, and J.-M. Esteva, Phys. Rev. B **33**, 4253 (1986).

[18] A. Fujimori, S. Suga, H. Negishi, and M. Inoue, Phys. Rev. B **38**, 3676 (1988).

[19] S. Watanabe and H. Kamimura, J. Phys. Soc. Jpn. **56**, 1078 (1987).

[20] K. Sato, Prog. Cryst. Growth Charact. **11**, 109 (1985).

[21] A. Fujimori, K. Terakura, M. Taniguchi, S. Ogawa, S. Suga, M. Matoba, and S. Anzai, Phys. Rev. B **37**, 3109 (1988).

[22] T. Mizokawa, H. Namatame, A. Fujimori, K. Akeyama, H. Kondoh, H. Kuroda, and N. Kosugi, Phys. Rev. Lett. **67**, 1638 (1991).

[23] A. Fujimori, N. Kimizuka, M. Taniguchi, and S. Suga, Phys. Rev. B **36**, 6691 (1987); parameter values for FeO are interpolated from those found from MnO (Ref. 3) and NiO (Ref. 4).

[24] A. Fujimori, M. Saeki, N. Kimizuka, M. Taniguchi, and S. Suga, Phys. Rev. B **34**, 7318 (1986).

[25] A. E. Bocquet, A. Fujimori, T. Mizokawa, T. Saitoh, H. Namatame, S. Suga, N. Kimizuka, Y. Takeda, and M. Takano, Phys. Rev. B **45**, 1561 (1992).

[26] G. H. Jonker and J. H. van Santen, Physica (The Hague) **16**, 337 (1950).

[27] S. Sugano, Y. Tanabe, and H. Kamimura, *Multiplets of Transition-Metal Ions in Crystals* (Academic, New York, 1970).

[28] A. Fujimori, H. Kino, H. Namatame, H. Negishi, and M. Inoue (unpublished).

[29] B. H. Brandow, Adv. Phys. **26**, 651 (1977); J. Kanamori, Prog. Theor. Phys. **30**, 275 (1963).

[30] Y. Tanabe and S. Sugano, J. Phys. Soc. Jpn. **9**, 766 (1954).

[31] D. W. Bullett, J. Phys. C **15**, 6163 (1982); M. A. Kahn, *ibid.* **9**, 81 (1976).

[32] Due to the complex coordination geometry of the pyrite-type structure and the partial filling of the ligand S 3*p* orbitals, there is no simple relationship between T_σ, T_π, $(pd\sigma)$, and $(pd\pi)$. We have utilized the fact that $3T_\pi^2+2T_\sigma^2$ is conserved for a rigid rotation of the S_6 octahedron (the cation is surrounded by six S atoms in the pyrites also) and that $T_\pi \approx 0$ as suggested from band-structure calculations (Ref. 31), in order to obtain an effective T_σ. The effect of the partial filling ($S^-:3p^5$) is included through a factor $\frac{5}{6}$ multiplying T_σ^2. Then, $2T_\sigma^2 \approx \frac{5}{6}\{3[\sqrt{3}(pd\sigma)]^2+2[2(pd\pi)]^2\}$, yielding T_σ.

[33] J. C. Fuggle, O. Gunnarsson, G. A. Sawatzky, and K. Schönhammer, Phys. Rev. B **37**, 1103 (1988).

[34] J. Zaanen and G. A. Sawatzky, Phys. Rev. B **33**, 8074 (1986).

[35] L. F. Mattheiss, Phys. Rev. B **5**, 290 (1972).

[36] K. Terakura, T. Oguchi, A. R. Williams, and J. Kübler, Phys. Rev. B **30**, 4734 (1984).

[37] A. Fujimori, M. Matoba, S. Anzai, K. Terakura, M. Taniguchi, S. Ogawa, and S. Suga, J. Magn. Magn. Mater. **70**, 67 (1987).

[38] K. Okada and A. Kotani, J. Electron Spectrosc. Relat. Phenom. **52**, 313 (1990).

[39] A. J. Wilson, Adv. Phys. **21**, 143 (1972).

[40] D. K. G. de Boer, C. Haas, and G. A. Sawatzky, Phys. Rev. B **23**, 4369 (1981).

[41] K. Okada and A. Kotani, J. Phys. Soc. Jpn. **60**, 722 (1991).

[42] K. Okada, A. Kotani, and B. T. Thole, J. Electron Spectrosc. Relat. Phenom. (to be published).

[43] After having completed the first version of the manuscript, the authors noticed a paper by G. Lee and S.-J. Oh [Phys.

Rev. B **43**, 14 674 (1991)], in which the metal 2p core-level XPS spectra of NiO, CoO, and FeO have been calculated by taking into account the anisotropic hybridization (different T_σ and T_π). They have thus obtained results in good agreement with ours, but their U and Δ values were chosen very differently between different experiments (core-level XPS, valence-band XPS, etc.) because the d-d exchange interaction has been differently included in U and Δ.